Scientific Research Publishing

Open Journal of Applied Sciences, 2026, 16(11), 4245-4267
https://www.scirp.org/journal/ojapps
ISSN Online: 2165-3925
ISSN Print: 2165-3917

Modeling and Analysis of an Airport Electrical System Using the Newton-Raphson Method

Anthony Bassesuka Sandoka Nzao[1*], Benjamin Ndubu Khonde[1], Tuka Biaba Samuel Garcia[2]

[1]Department of Electrical Engineering, ISTA Kinshasa, Kinshasa, Democratic Republic of the Congo
[2]Department of Science and Technology/Electrical Engineering, Doctoral School of ISTA Kinshasa, Kinshasa, Democratic Republic of the Congo
Email: *bass_sandoka@yahoo.fr, benjamin.ndubu@gmail.com, tukasamuel23@gmail.com

How to cite this paper: Nzao, A.B.S., Khonde, B.N. and Garcia, T.B.S. (2026) Modeling and Analysis of an Airport Electrical System Using the Newton-Raphson Method. *Open Journal of Applied Sciences*, **16**, 4245-4267.
https://doi.org/10.4236/ojapps.2026.1611231

Received: August 31, 2026
Accepted: October 30, 2026
Published: November 2, 2026

Copyright © 2026 by author(s) and Scientific Research Publishing Inc.
This work is licensed under the Creative Commons Attribution International License (CC BY 4.0).
http://creativecommons.org/licenses/by/4.0/

Open Access

Abstract

The energy resilience of critical airport infrastructure poses a major systemic challenge, particularly in developing environments where national power grids are structurally unstable. This paper presents a mathematical modelling and quantitative analysis of the electrical supply security of an airport hub, using Ndjili International Airport in Kinshasa, DR Congo, as an empirical anchor. The proposed approach formalizes the interdependence among primary power sources, internal distribution architecture, critical load behaviour, and backup system dynamics. Methodologically, the research integrates on-site characterization with a power flow calculation model solved via the Newton-Raphson iterative algorithm, enabling an assessment of network robustness against contingencies. Numerical simulations highlight the topological vulnerabilities of the current system and quantify the impact of recurrent outages on reliability indicators. Finally, this paper demonstrates the efficacy of active and passive redundancy strategies, specifically through the integration of dedicated transformers and synchronous diesel generators and formulates a techno-economic optimization framework aimed at maximizing service continuity and compliance with international aviation safety standards.

Keywords

Airport Microgrid, Power Flow, Newton-Raphson Algorithm, Systemic Reliability, Topological Redundancy, Energy Resilience

1. Introduction

Airport electrical infrastructures represent critical industrial systems, whose operational governance demands absolute availability, heightened resilience, and an optimal safety threshold [1]-[3]. These imperatives are fundamental to ensuring

the continuity of flight operations, Airfield Ground Lighting (AGL), and the power supply of emergency communication and navigation systems [4] [5]. According to the literature presented by [6] [7], in environments characterized by structural instability of the public bulk power system, the integration of alternative energy sources and emergency systems becomes a systemic imperative to mitigate primary grid failures [8] [9].

Ndjili International Airport (IATA: FIH, ICAO: FZAA) [10], the primary aviation hub of the Democratic Republic of the Congo located in Kinshasa, perfectly illustrates these challenges of energy vulnerability. Despite its strategic role in national and international air traffic, this infrastructure has experienced several critical power supply disruptions [10]-[13]. Notably, prolonged major outages have impacted the control tower and runway visual aids, thereby compromising the safety of landing phases and inducing significant operational disruptions alongside rigorous administrative investigations [12].

In response to these contingencies, this study develops a comprehensive systemic modeling of the airport's electrical network. Through the application of the iterative Newton-Raphson method, this work aims to analyze the infrastructure's performance under steady-state and dynamic regimes, while evaluating the efficacy of the configured redundancy strategies. Finally, this research highlights the technological bottlenecks and control-loop challenges associated with the integration of backup systems, which are essential to guaranteeing the infrastructure's energy sovereignty against the disturbances of the national interconnected grid.

2. Method

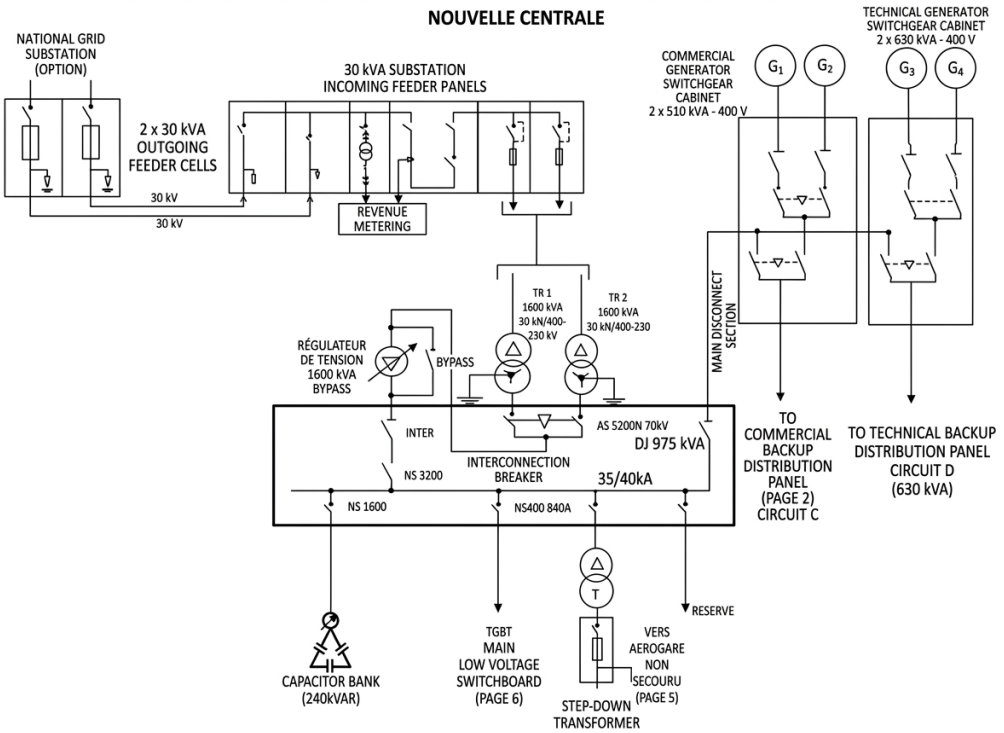
2.1. Power Context of Ndjili Airport

Historically, the electrical power supply of Ndjili International Airport has depended on the Congolese national grid, managed by the *Société Nationale d'Électricité* (SNEL) [10]-[13]. Faced with recurrent blackouts of the public utility grid most notably during the disruptions of September 2025 the airport experienced protracted outage periods that paralyzed critical operations, including runway systems, Airfield Ground Lighting (AGL), and control tower functionalities [10]-[13]. To mitigate these systemic failures, a new *15 MVA* transformer was recently commissioned on-site to enhance power supply stability and attenuate reliance on the surrounding domestic distribution grid [10]-[13]. The structural and consumption data used to configure this model were derived from an on-site characterisation campaign conducted in collaboration with the Régie des Voies Aériennes and SNEL in October 2025. Measurements of rated power and load profiles for critical loads were obtained using Class A power quality analysers recording at 15-minute intervals at the main low-voltage distribution boards serving the terminal, the control tower, and the airfield lighting system. Cable parameters for *95* to *240* mm^2 copper conductors with XLPE insulation and transformer leakage impedances *TR1 and TR2* were sourced directly from manufacturer datasheets validated during the installation of the new *15 MVA* transformer. Historical fault occurrences

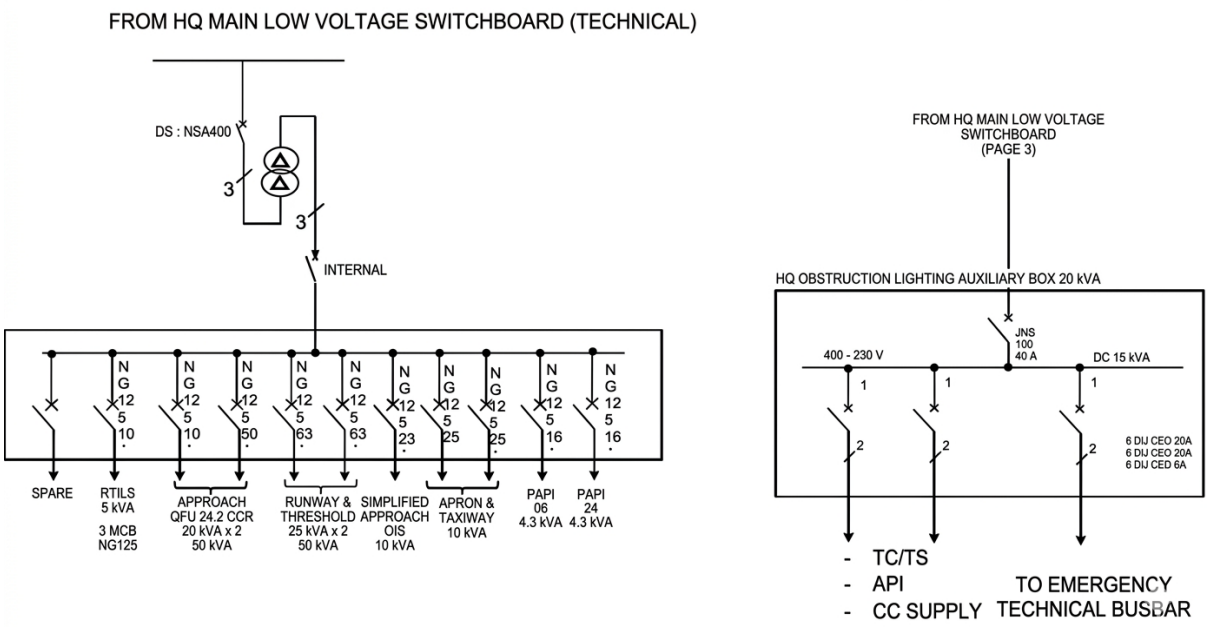
and timelines are based on control tower operational logs and technical incident reports from September *2025*.

2.2. Global Schematic of the Ndjili International Airport Electrical System

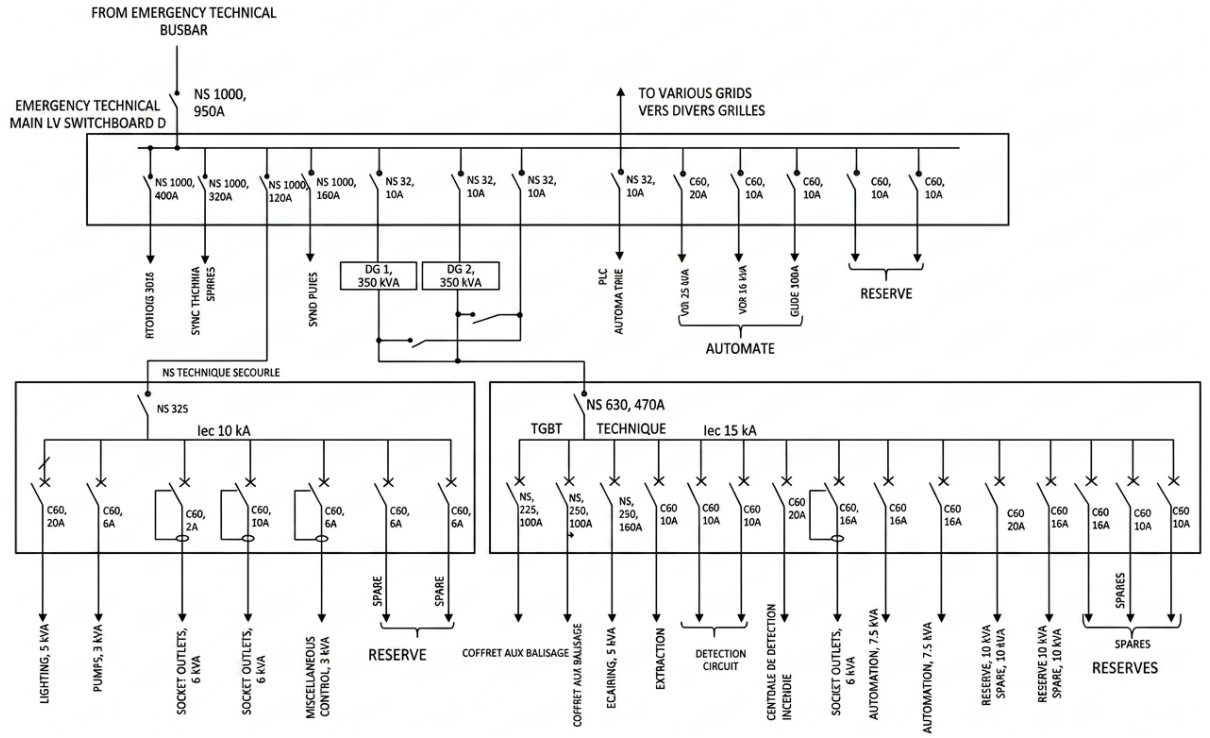
As illustrated in **Figures 1(a)-(c)**, the primary electrical power supply of Ndjili International Airport is delivered by two *1600 kVA* transformers operating in a redundant configuration. Emergency backup power for the technical facilities is provided by two alternating *635 kVA* diesel generator units. Additionally, a *350 kVA* generator ensures backup power for the commercial sector [10]. Voltage regulators and Uninterruptible Power Supplies (UPS) are integrated into the network architecture to enhance the reliability of the airfield ground lighting circuits, as well as the power supply lines for navigation and communication equipment. For security and safety imperatives, the comprehensive global electrical schematic of Ndjili International Airport cannot be disclosed to the public [13]. The backup architecture modelled for the numerical simulations comprises three distinct diesel generation units (*G1*, *G2*, *G3*), distributed according to the hub's active and apparent power requirements. Although the preliminary schematic (**Figure 1(a)**) shows cabinets configured for theoretical coupling arrangements, commercial cabinet: $2\times 510\,kVA$; technical cabinet: $2\times 630\,kVA$, the mathematical simulation model is based on the actual physical distribution measured at the backup switchboard (**Table 1**), ensuring a total available nominal capacity of *1428 kW* at *1785 kVA* and $\cos\varphi = 0.8$:



(a)



(b)



(c)

Figure 1. Functional block diagram of the Ndjili Airport electrical system: public utility grid, power transformers, MV/LV transformers, distribution lines, backup generators, critical and non-critical loads [10] [11]. (a) Topology of SNEL power sources and emergency backup generator circuits [10]-[13]; (b) HQ LVMSB topology and emergency backup generator circuits [10]-[13]; (c) Topology of critical loads powered by emergency backup generators.

- Generator 1 (*G1*): Nominal active power of P_{n1} = 280 kW, apparent power of *350 kVA*; primarily dedicated to partial backup for airfield lighting and the

control tower.

- Generator 2 (*G2*): Nominal active power of P_{n2} = 508 kW, apparent power of *635 kVA*; assigned to the aeronautical technical auxiliaries busbar.
- Generator 3 (*G3*): Nominal active power of P_{n3} = 640 kW, apparent power of *800 kVA*; sized to handle the residual load of the backed-up commercial terminal.

2.3. Airport Electrical System Modeling

The mathematical modeling of an airport electrical system aims to represent the dynamic and static behavior of the network to enable performance analysis and perturbation simulation. The primary components of the airport electrical system can be classified into three distinct subsystems [14]-[16]:

- Generation (generators);
- Transmission and distribution (lines);
- Demand (consumers).

To analyze a complex electrical power network such as an airport electrical system, equivalent models or schematics of these core components, namely generators, various types of transformers, lines, and loads, are established.

In addition to the aforementioned aspects, several other concepts are addressed, specifically [14]-[16]:

- Power balance equations;
- Probabilistic approaches to reliability;
- Redundant configuration frameworks.

2.3.1. Alternator Model

To model the emergency diesel generator, the unit is represented by an internal voltage source E_g in series with an internal impedance Z_g. The dynamic model of the Automatic Voltage Regulator (AVR), utilized to simulate the transient response during utility grid outages, can be formulated via the following equation [17]:

$$E_g = Z_g \times I_L + V_t \tag{1}$$

$$Z_g = R_g + jX_g \tag{2}$$

The AVR adjusts the generator's excitation voltage to maintain a constant terminal voltage. The standard first-order model (modified IEEE Type 1) is expressed by the following differential equation [14]-[16]:

$$\frac{\mathrm{d}E_g}{\mathrm{d}t} = \frac{1}{T_A}\left[K_A\left(v_{res} - v_f\right) - E_g\right] \tag{3}$$

where:

- E_g : Generator internal voltage (V).
- T_A : Regulator time constant (s), typically between 0.02 and 0.1 s.
- K_A : Regulator gain, typically between 20 and 100.
- v_{res} : Desired reference voltage (V).

- v_f : Measured voltage at the generator terminals (V).

During a grid outage, the load switches to the generator. The terminal voltage V_t drops instantaneously due to the internal impedance Z_g. The instantaneous algebraic relationship is given by:

$$V_t = E_g - Z_g \times I_L \tag{4}$$

- I_L : Current drawn by the emergency load (A).
- Z_g : Transient impedance $R_g + jX'_d$, where jX'_d represents the direct-axis transient reactance.

The generator is considered the core of the airport electrical system, ensuring the production of the electrical energy demanded by the consumer. In power flow analysis, the generator is modeled as a constant voltage source V_g injecting active power P_g and reactive power Q_g (as illustrated in Figure 2).

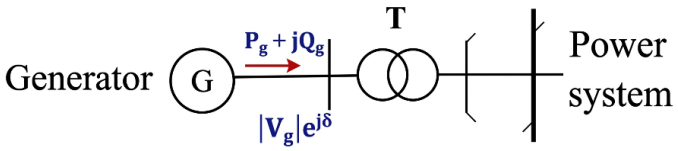


Figure 2. Generator modeling [14].

The reactive power of the generator is adjusted to maintain a constant bus voltage. Furthermore, the generator is characterized by two reactive power operational limits, namely Q_{gmax} and Q_{gmin}. When either of these boundaries is reached, the reactive power Q remains fixed at that limiting value, and the bus voltage is no longer strictly regulated.

2.3.2. Transmission and Distribution Line Modeling

In modeling the electrical lines of an airport power system, the selection of the appropriate model depends on the cable length and the specific objective of the simulation (steady-state or transient analysis). Airport networks predominantly utilize underground cables operating at Medium Voltage (MV: 15 kV or 20 kV) and Low Voltage (LV: 400 V), which are characterized by short distances, typically under 10 km.

The standard representation for these distances is the nominal π equivalent circuit model (applicable to short and medium lines, as illustrated in Figure 3).

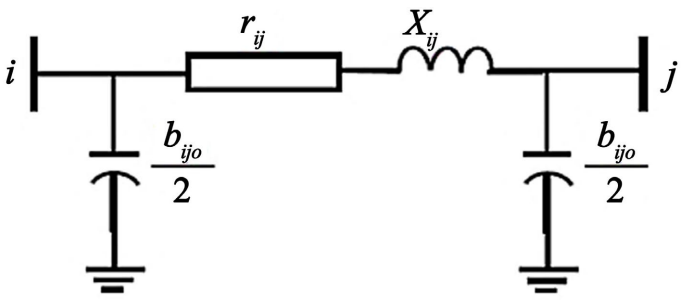


Figure 3. Transmission and distribution line modeling [15].

The nodal admittance matrix of a transmission line connecting bus i to bus j is given by [14]-[16]:

$$\begin{cases} \underline{Y} = \begin{pmatrix} y_{ij} + \dfrac{y_{ij0}}{2} & -y_{ij} \\ -y_{ij} & y_{ij} + \dfrac{y_{ij0}}{2} \end{pmatrix} \\ \underline{y}_{ij} = \dfrac{1}{r_{ij} + jx_{ij}} = g_{ij} - jb_{ij} \\ \underline{y}_{ij0} = jb_{ij0} \end{cases} \tag{5}$$

where r_{ij} is the series resistance of the line, r_{ij} is the series reactance of the line, and b_{ij0} represents the shunt susceptance.

Each transmission line or underground cable is defined per kilometer by four primary electrical parameters:

- R: Linear resistance (Ω/km) modeling Joule losses.
- L: Linear inductance (H/km) yielding the inductive reactance ($X = \omega L$).
- C: Linear capacitance (F/km) modeling the capacitive charging effect, which is highly pronounced in airport underground cables.
- G: Linear conductance (S/km) modeling dielectric losses, typically neglected in analysis ($G \approx 0$).

2.3.3. Transformer Model

An electrical power transformer is mathematically represented by an asymmetrical π equivalent two-port network. The associated operational parameters are the transformation ratio a and the leakage impedance [14]-[16]. The ratios ($a = R_{ij}/R$) are integrated directly into the elements of the bus admittance matrix. Consequently, the matrix susceptance components ($b = R_{ij}$) are formulated as functions of the transformation ratios a (as illustrated in **Figure 4**).

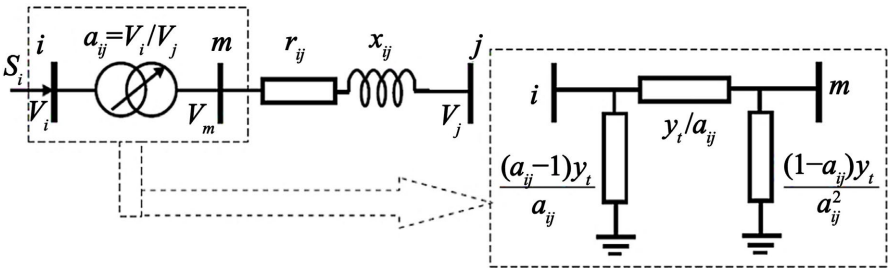


Figure 4. Transformer model [14] [16]-[19].

The admittance matrix of a transformer connected between bus i and bus j is expressed as:

$$Y = \begin{pmatrix} \dfrac{1}{a^2} y_{ij} & -\dfrac{1}{a} y_{ij} \\ -\dfrac{1}{a} y_{ij} & y_{ij} \end{pmatrix} \tag{6}$$

where:

- *a:* The transformation ratio.
- y_{ij} : The admittance of branch *i-j*.

In specific cases, the magnetizing branch is incorporated into the model, where it is represented as a shunt inductive susceptance [14]-[16].

The MV/LV transformers are modeled by their equivalent impedance $Z_t = R_t + jX_t$, which accounts for the internal voltage drop and associated power losses. The secondary voltage is calculated by [14]-[16]:

$$V_{sec} = V_{prim} \cdot \frac{N_{sec}}{N_{prim}} - I_{sec} Z_t \tag{7}$$

where: N_{prim} and N_{sec} represent the primary and secondary number of turns, respectively.

2.3.4. Electrical Load Modeling

The electrical load is commonly modeled as a load impedance Z_{load} that consumes constant active power P_L and reactive power Q_L (as illustrated in **Figure 5**) [14]-[16].

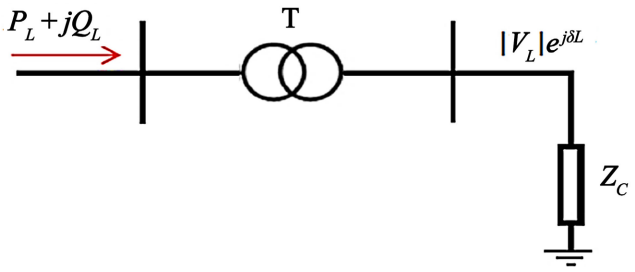


Figure 5. Electrical load model [14]-[16].

The loads within the airport electrical system are classified into two categories:

Critical loads (runway lighting, control tower, airfield ground lighting, communication systems):

Represented as constant power loads $P + jQ$ or by functions dependent on the voltage V^{α} and the power factor, where α describes the sensitivity of the load to voltage fluctuations [14]-[17].

$$P_{critique}(V) = P_0 \left(\frac{V}{V_0} \right)^{\alpha} \tag{8}$$

$$Q_{critique}(V) = Q_0 \left(\frac{V}{V_0} \right)^{\beta} \tag{9}$$

The introduction of α and β coefficients near unity [0.9, 1.1] indicates that the critical loads exhibit a behavior approximating a constant current characteristic.

- If ($\alpha = \beta = 0$): The load exhibits a constant power characteristic (independent of *V*). This applies to modern electronic equipment equipped with switch-mode

power supplies (control tower servers, radar systems, telecommunication switches) that regulate and enforce their internal power consumption.

- If ($\alpha = \beta = 1$): The load exhibits a constant current characteristic. The specified intervals [0.9, 1.1] accurately model modern LED airfield ground lighting or legacy systems driven by Constant Current Regulators (CCRs), which maintain a stable current despite network voltage fluctuations.
- If ($\alpha = 2$ or $\beta = 2$): The load would exhibit a constant impedance characteristic (e.g., resistive heating elements).

Non-critical loads (administrative buildings, commercial areas, logistical zones):

Modeled as constant or voltage-dependent loads, integrated with automated load shedding capabilities in the event of power deficits.

For administrative buildings and commercial zones, the load behavior is frequently modeled as Constant Power ($\alpha = \beta = 0$) or via a classical polynomial ZIP model. The defining operational feature here lies in the Under-Frequency or Under-Voltage Automatic Load Shedding (ALS) logic function. Mathematically, the non-critical load configuration is expressed as [17]-[21]:

$$P_{non\text{-}critique}(V,f,t) = S(t) \times P_{0_nc} \left(\frac{V}{V_0} \right)^{\alpha_{nc}} \tag{10}$$

$$Q_{non\text{-}critique}(V,f,t) = S(t) \times Q_{0_nc} \left(\frac{V}{V_0} \right)^{\beta_{nc}} \tag{11}$$

where $S(t) \in (0,1)$ is a binary state variable governed by a protective relaying function:

- Under-Frequency Load Shedding (UFLS): If the emergency generator frequency drops below a predefined threshold (e.g., f < 48.5 Hz) due to mechanical overloading of the diesel engine, then $S(t) = 0$.
- Under-Voltage Load Shedding (UVLS): If the measured voltage V remains below a critical threshold (e.g., 0.85 pu) for more than x milliseconds (implying the AVR fails to provide adequate compensation), then $S(t) = 0$.

By synthesizing the generator model (E_g, Z_g), the nominal π-line models (Z_{ligne}, Y_{ligne}), and the two distinct load categories, the power balance equation at the airport bus is formulated as follows:

$$P_{totale}(V) = P_0 \left(\frac{V}{V_0} \right)^{\alpha} + S(t) \times P_{0_nc} \left(\frac{V}{V_0} \right)^{\alpha_{nc}} \tag{12}$$

$$Q_{totale}(V) = Q_0 \left(\frac{V}{V_0} \right)^{\beta} + S(t) \times Q_{0_{nc}} \left(\frac{V}{V_0} \right)^{\beta_{nc}} - Q_{capacitif_lignes}(V) \tag{13}$$

2.3.5. Load Shedding Relay Modeling (UFLS/UVLS)

The automatic load shedding of non-critical loads is triggered based on voltage and frequency threshold logic. The equation governing the control variable $S(t)$ is formulated as [19] [20]:

$$S(t)=\begin{cases}0 \text{ if } f(t)\le f_{threshold} \text{ for } \Delta t_f \text{ (Uder-Frequency Laod shedding)}\\ 0 \text{ if } V(t)\le V_{threshold} \text{ for } \Delta t_v \text{ (Uder-Voltage Laod shedding)}\\ 1 \text{ Otherwise (Operation Normal)}\end{cases} \quad (14)$$

Recommended values for an airport emergency power system:

- Frequency threshold $f_{threshold}$ = 48.5 Hz (for a 50 Hz grid) with an operating time Δt_f = 100 ms.
- Voltage threshold $V_{threshold}$ = 0.85 pu with a time delay Δt_v = 500 ms (allowing adequate time for AVR response).

Unlike critical loads $\alpha, \beta \approx 1$, the terminal administrative buildings and commercial areas integrate numerous Heating, Ventilation, and Air Conditioning (HVAC) systems, computer terminals, and commercial lighting [19] [20].

The standardized values used to model these logistical zones are given by [19] [20]:

- α_{nc} = 0.25 to 0.50 (mixed behavior between constant power and constant current, induced by air conditioning compressors).
- β_{nc} = 1.50 to 2.50 (highly inductive and voltage-dependent behavior, characteristic of fan and pump motors).

Logic Mechanism of the Load-Shedding Relay

Automatic shedding of non-critical and semi-critical loads is controlled by a binary signal $S(t)\in\{0,1\}$, as shown in Equation (13). This process uses instant on/off switching by opening motorised circuit breakers, such as the *NS1600* in **Figure 1(a)**, after time delays of *100 ms* or *500 ms*. The physical relay does not allow for gradual reduction; it only switches fully on or off.

While the circuit breaker works with simple on/off logic $S(t) = 0$, in reality, the loads decrease gradually due to the dynamic damping in the *ZIP* load model after disconnection. The nodal voltage drops steadily as line capacitances discharge and tertiary motors, like terminal *HVAC* units, release *back-EMF*. The absorbed power then declines along a curve set by the voltage exponents until the voltage at the disconnected node reaches zero.

2.4. Numerical Power Flow Resolution

The mathematical formulation of the airport electrical system investigated in this paper is governed by the power flow (Load Flow) equations adapted for an *n*-bus power network. These equations express the active power P_i and reactive power Q_i injected at bus *i* as a function of the elements of the bus admittance matrix [Y_{bus}], defined as follows [19] [20]:

$$Y_{ij} = G_{ij} + jB_{ij} \quad (15)$$

In this formulation, the bus voltages are expressed in polar coordinates by their magnitude V and phase angle θ. The phase angle difference between two buses is denoted as $\theta_{ij} = \theta_i - \theta_j$. The general power flow equations for each bus i ($i = 1, 2, \cdots, n$) are formulated as follows [17]-[20]:

$$\begin{cases} P_i = V_i \sum_{j=1}^{n} V_j \left[G_{ij} \cos\left(\theta_i - \theta_j\right) + B_{ij} \sin\left(\theta_i - \theta_j\right) \right] \\ Q_i = V_i \sum_{j=1}^{n} V_j \left[G_{ij} \sin\left(\theta_i - \theta_j\right) + B_{ij} \cos\left(\theta_i - \theta_j\right) \right] \end{cases} \quad (16)$$

where:

- V_i and V_j represent the Root-Mean-Square (RMS) voltage magnitudes at buses *i* and *j*, respectively.
- G_{ij} and B_{ij} are the conductance and susceptance elements of the transmission line connecting bus *i* and *j*.
- $\theta_{ij} = \delta_i - \delta_j$ denotes the phase angle difference.
- *n* represents the total number of network buses.

This formulation is widely preferred for the Newton-Raphson method because it directly aligns with the operational specifications of PV buses (where the voltage magnitude V is maintained constant by the emergency backup generator's AVR) [18] [20].

To resolve the airport electrical power outage problem and guarantee both the stability and continuity of the airport's priority loads, the system of power flow Equation (16) for P_i, Q_i is coupled with the previously defined voltage-dependent load models (refer to Equations (8) - (13)). For the airport load bus (denoted as bus *i*), the net power injections are formulated as [18] [20]:

$$\begin{cases} P_{injecte,i} = P_{critique,i}\left(V_i\right) - S\left(t\right) \cdot P_{non_{critique},i}\left(V_i\right) \\ Q_{injecte,i} = Q_{critique,i}\left(V_i\right) - S\left(t\right) \cdot Q_{non\text{-}critique,i}\left(V_i\right) \end{cases} \quad (17)$$

The Newton-Raphson algorithm aims to eliminate the mismatch between the net scheduled power injections and the calculated powers derived from Equation (16).

To incorporate voltage-dependent load models into the Newton-Raphson formulation, the conventional Jacobian matrix must be modified. Static loads uniquely alter the diagonal elements of the Jacobian, as the power consumed at bus *i* is independent of the voltage magnitude or phase angle of any other bus *j* [19] [20].

The iterative linear system of the Newton-Raphson method is expressed as [17] [20]:

$$\begin{bmatrix} \Delta P \\ \Delta Q \end{bmatrix} = \begin{bmatrix} H & N \\ M & L \end{bmatrix} \begin{bmatrix} \Delta\theta \\ \Delta V/V \end{bmatrix} \quad (18)$$

where the submatrices represent the partial derivatives of the power mismatches [16] [20]:

$$\begin{cases} \Delta P_i = P_{g,i} - P_{charge,i}\left(V_i\right) - P_i\left(\theta, V\right) \\ \Delta Q_i = Q_{g,i} - Q_{charge,i}\left(V_i\right) - Q_i\left(\theta, V\right) \end{cases} \quad (19)$$

For $\neq i$, the elements of the Jacobian matrix $\begin{bmatrix} H & N \\ M & L \end{bmatrix}$ depend exclusively on the network topology, as defined by the bus admittance matrix Y_{bus} [18] [20].

$$\begin{cases} H_{ij} = \dfrac{\partial P_i}{\partial \theta_j} = V_i V_j \left[G_{ij} \sin\left(\theta_i - \theta_j\right) - B_{ij} \cos\left(\theta_i - \theta_j\right) \right] \\ N_{ij} = V_j \dfrac{\partial P_i}{\partial V_j} = V_i V_j \left[G_{ij} \cos\left(\theta_i - \theta_j\right) + B_{ij} \sin\left(\theta_i - \theta_j\right) \right] \\ M_{ij} = \dfrac{\partial Q_i}{\partial \theta_j} = -V_i V_j \left[G_{ij} \cos\left(\theta_i - \theta_j\right) + B_{ij} \sin\left(\theta_i - \theta_j\right) \right] = -N_{ij} \\ L_{ij} = V_j \dfrac{\partial Q_i}{\partial V_j} = V_i V_j \left[G_{ij} \cos\left(\theta_i - \theta_j\right) - B_{ij} \sin\left(\theta_i - \theta_j\right) \right] = H_{ij} \end{cases} \tag{20}$$

The modified diagonal elements for bus i incorporate the load parameters α, and β (for critical loads), as well as α_{nc} and β_{nc} (for non-critical loads), along with the load shedding control factor $S(t)$.

A. Derivatives with Respect to Phase Angle θ_i

Since the phase angle has no influence on static voltage-dependent loads, the analytical expressions remain identical to the conventional load flow formulation [19] [20]:

$$\begin{cases} H_{ii} = \dfrac{\partial P_i}{\partial \theta_i} = Q_i\left(\theta, V\right) - B_{ii} V_i^2 \\ M_{ii} = \dfrac{\partial Q_i}{\partial \theta_i} = P_i\left(\theta, V\right) - G_{ii} V_i^2 \end{cases} \tag{21}$$

B. Derivatives with Respect to Voltage Magnitude (V_i) Impact of Electrical Loads

The voltage dependence of the loads adds a direct subtractive term onto the diagonal elements of the (N) and (L) submatrices. Utilizing the standardized formulation $V_i \dfrac{\partial}{\partial V_i}$ [16]-[36]:

$$\begin{cases} N_{ij} = V_i \dfrac{\partial \Delta P_i}{\partial V_i} = \left[P_i\left(\theta, V\right) - G_{ii} V_i^2 \right] - \left[\alpha P_{0,i} \left(\dfrac{V_i}{V_0} \right)^{\alpha} + S(t) \times \alpha_{nc} P_{0_{nc},i} \left(\dfrac{V_i}{V_0} \right)^{\alpha_{nc}} \right] \\ L_{ii} = V_i \dfrac{\partial \Delta Q_i}{\partial V_i} = \left[Q_i\left(\theta, V\right) - B_{ii} V_i^2 \right] - \left[\beta Q_{0,i} \left(\dfrac{V_i}{V_0} \right)^{\beta} + S(t) \times \beta_{nc} Q_{0_{nc},i} \left(\dfrac{V_i}{V_0} \right)^{\beta_{nc}} \right] \end{cases} \tag{22}$$

Static-Dynamic Digital Coupling

The digital workflow combines steady-state power flow calculation (spatial load flow) and transient time-domain simulation according to the following algorithmic sequence:

1) Initialisation: The Newton-Raphson algorithm solves the nonlinear algebraic Equation (15) for $t < 5.0$ s under a strict convergence tolerance of $e = 10^{-6}$ pu on residuals DP and DQ. The calculated voltage moduli and initial angles determine the internal state (E_{g0}, v_{f0}) of the alternating generators.

2) Handling reactive power limits: At each Newton-Raphson iteration, if the calculated reactive power of an alternator exceeds Q_{gmax} or Q_{gmin}, the corresponding PV-type node is immediately converted to a PQ node with Q_{limit}. The voltage

is then released and recalculated as a free system variable until convergence.

3) Switching event $t = 5.0$ s: The failure of the main network instantaneously modifies the topology of the nodal admittance matrix $[Y_{bus}]$, isolating the source node *N1*. The differential equations of the alternator (3) and the frequency response (25) are then activated in closed loop.

4) Time integration: The transient dynamics are solved using the modified Euler numerical method (or 4th-order Runge-Kutta) with a fixed time step $Dt = 1$ ms, ensuring numerical stability against the stiffness of the AVR time constants $T_A = 0.05$ s *and the mechanical* constants. At each time step, the binary load shedding variable $S(t)$ is evaluated.

2.5. Reliability Analysis under Component Failures

Network reliability is modeled through the availability probability $R(t)$ of the individual components [37]:

$$R(t) = \mathrm{e}^{-\lambda t} \tag{23}$$

where λ represents the failure rate of the specific component (transformer, transmission line, or generator). The overall system reliability performance is obtained by combining components in series or parallel configurations [37]:

Series Configuration:

$$R_{sys}(t) = \prod_{i=1}^{n} R_i(t). \tag{24}$$

Parallel Configuration (Redundant):

$$R_{sys} = 1 - \prod_{i=1}^{n} \left[1 - R_i(t)\right] \tag{25}$$

This analytical framework enables quantifying the direct impact of emergency backup generators and transformer redundancy on service continuity within the airport infrastructure.

2.6. System Frequency Response Model

The transient temporal response of the network frequency (typically following a load disturbance incident or alternator startup) mathematically corresponds to the step response of an underdamped second-order system, characterized by decaying pseudo-periodic oscillations. This linear second-order dynamic behavior is governed by the following canonical differential equation, expressed in terms of the frequency state variable $f(t)$ [20].

$$\frac{\mathrm{d}^2 f(t)}{\mathrm{d}t^2} + 2\zeta\omega_n \cdot \frac{\mathrm{d}f(t)}{\mathrm{d}t} + \omega_n^2 \cdot f(t) = \omega_n^2 \cdot f_\infty \tag{26}$$

3. Simulation Results

3.1. Simulation Parameters

Table 1 below summarises all the numerical parameters injected into the simulation code.

Table 1. Simulation parameters.

Parameters Category	Mathematical/Physical Parameter	Modeled Value (up or IF)
Network Foundations	Base power (S_{base})/Base voltage (V_{base})/ Nominal frequency (f_0)	5 MVA/400 V (LV) and 30 kV (HT) 50 Hz
Line Impedances	R: resistance, X: reactance of LV cables and B average transverse capacitive susceptibility	R = 0.012 pu, X = j0.008 pu and B = 0.004 pu
TR MV/BT Impedances	Short-circuit impedance (Z_t) for 1600 kVA *Nominal* transformation ratio (a)	Z_t = 0.005 + j0.060 pu, U_{cc} = 6% and U_n = 30 kV/400 V
Load Coefficients	Critical loads (Runway, Tower): α_c, β_c Non-critical loads (Shops): α_{nc}, β_{nc}	1.0, 1.0 (Constant Current CCR) 0.25, 1.50 (Tertiary ZIP Model)
Limits Generators	Reactive power: Q_{gmin}/ Q_{gmax}	−0.2 pu/+0.6 pu
Dynamic & AVR	Equivalent inertia constant of the diesel engine block H AVR regulator gain K_A/Time constant T_A	2.5 s 50.0/0.05 s
Cruise Control	Permanent static R_s/Actuator time constant τ_g	4%/0.15 s

3.2. Simulation Scenarios

Three primary operational scenarios were simulated in this study using the Python programming language:

1) Normal steady-state operation (stable public utility grid).

2) Public utility grid outage with automatic transfer to backup emergency sources (diesel generator sets).

3) Simultaneous failure of the public grid and a critical backup generator.

3.3. Steady-State Power Flow Distribution

Under normal steady-state conditions, the primary utility network supplies all electrical loads. The power balance demonstrates that critical loads consume a significant portion of the total energy. Table 2 and Figure 6 summarize these steady-state findings.

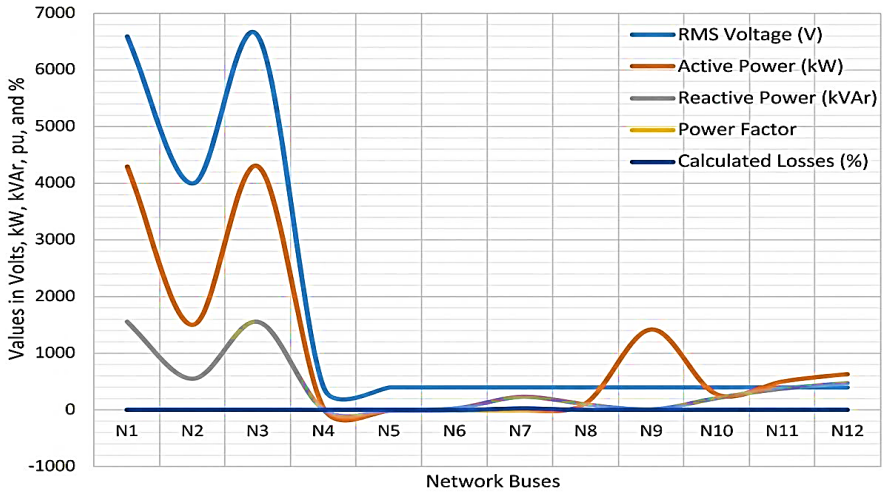


Figure 6. Power curves at the nodes of the Ndjili Airport electrical network.

Table 2. Power balance across different network buses under steady-state operation (Ndjili Airport).

Network Bus	Circuits/Subsystems	RMS Voltage (V)	Active Power (kW)	Reactive Power (kVAr)	Power Factor	Calculated Losses (%)
N1	Main SNEL Input HV Bus	6600	4300	1550	0.94	0.01
N2	Primary MV/LV Transformer	4000	1504	544	0.94	1.2
N3	Central MV Distribution Board	6600	4300	1550	1.00	0.01
N4	Critical Load-Airfield Ground Lighting	400	30	0	0.90	1.50
N5	Critical Load-Control Tower	400	8.99	3.252	0.90	1.00
N6	Semi-critical Load-Operational Buildings	400	51.81	18.74	0.90	0.80
N7	Non-critical Loads-Commercial & Services	400	623.8	225.66	0.80	10.00
N8	UPS + Battery Systems (Distributed Load)	400	128	94.4	0.80	2.5
N9	Emergency Diesel Generators (Total Capacity)	400	1428	1053.15	0.80	2.50
N10	Diesel Generator Unit 1	400	280	206.5	0.80	2.50
N11	Diesel Generator Unit 2	400	508	374.65	0.80	2.50
N12	Diesel Generator Unit 3	400	640	472	0.80	2.50

3.4. Grid Response under Perturbations

The primary utility network outage scenario was simulated to evaluate the dynamic performance of the emergency backup systems (as illustrated in Figure 7).

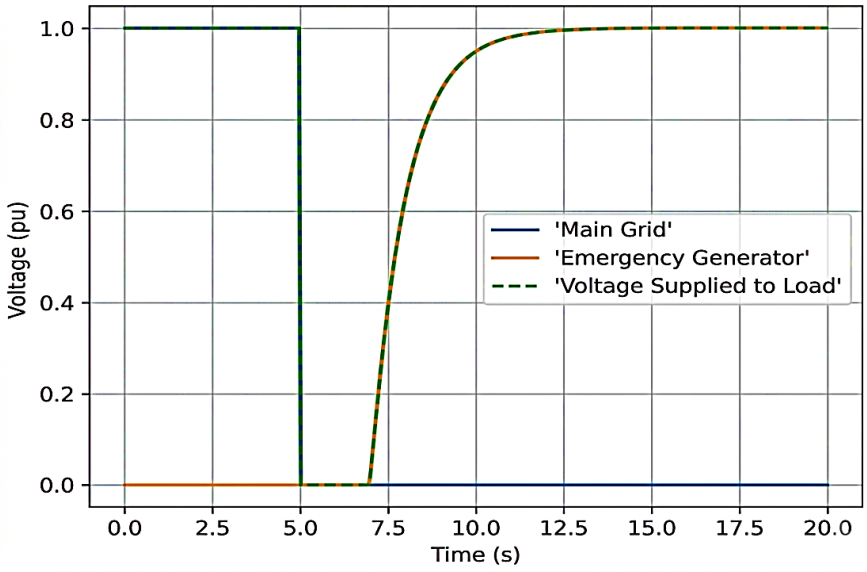


Figure 7. Transient voltage evolution during a main grid outage with transition to backup generators.

3.5. Simultaneous Failure: Main Grid and Backup System

This scenario, illustrated in Figure 8, represents an extreme condition where both the main power grid and a backup unit fail simultaneously.

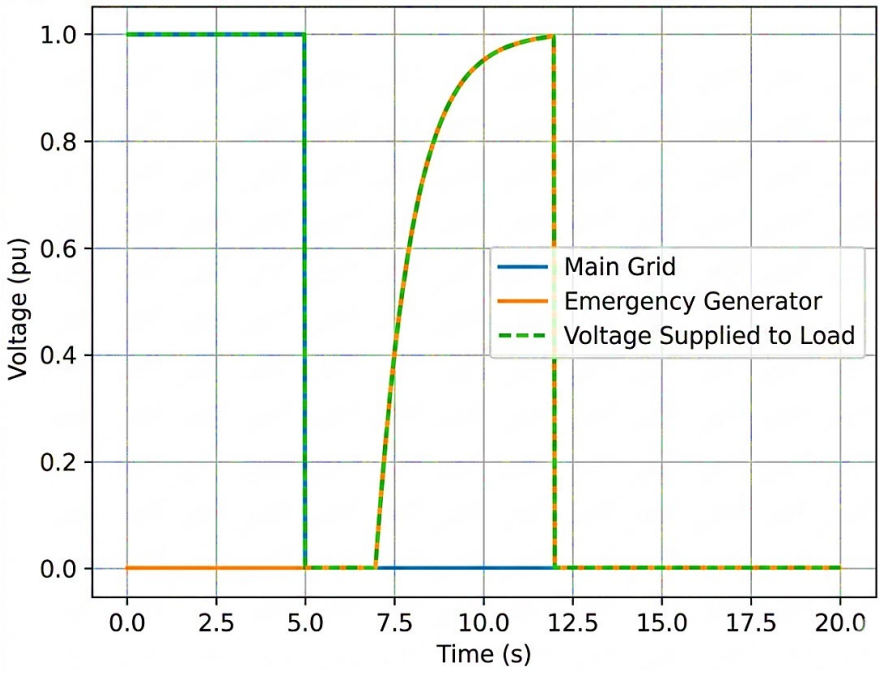


Figure 8. Simulation of a simultaneous main grid and backup generation failure.

3.6. System Frequency Behavior

Frequency analysis constitutes a fundamental indicator of the dynamic stability of a power system, particularly within critical infrastructures such as airports. Figure 9 illustrates the time evolution of the system frequency following a combined failure of the main grid and a backup source.

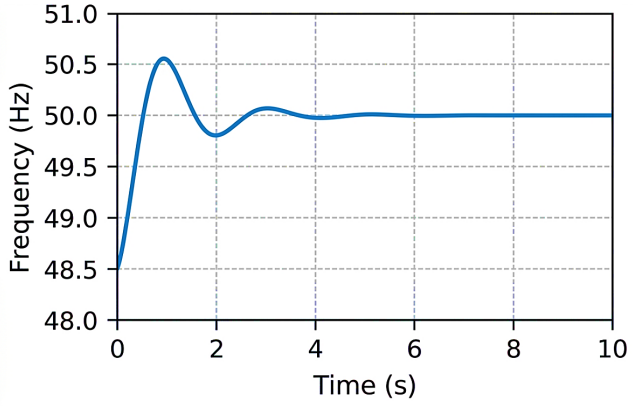


Figure 9. System frequency analysis following a failure.

3.7. Load Shedding Strategy

The load shedding strategy constitutes an essential mechanism to preserve power system stability in the event of a generation deficit. Figure 10 presents the power consumption evolution across different load categories (critical, semi-critical, and non-critical) during a major failure scenario.

Based on the steady-state energy balance presented in Table 1, the transient

scenario illustrated in Figure 10 was normalised using an equivalent local load of *100 kW*. The initial values at $t = 0$ s pertain to a specific section of the backed-up technical sub-distribution panel subject to a local overload. This approach allows for the evaluation of the relay's dynamic behaviour on a consistent relative scale and does not represent the airport's total cumulative load shown in Table 1. The curvilinear decrease in non-critical power confirms the relationship between the relay's binary state $S(t) = 0$ and the voltage response calculated by the *ZIP* polynomial model.

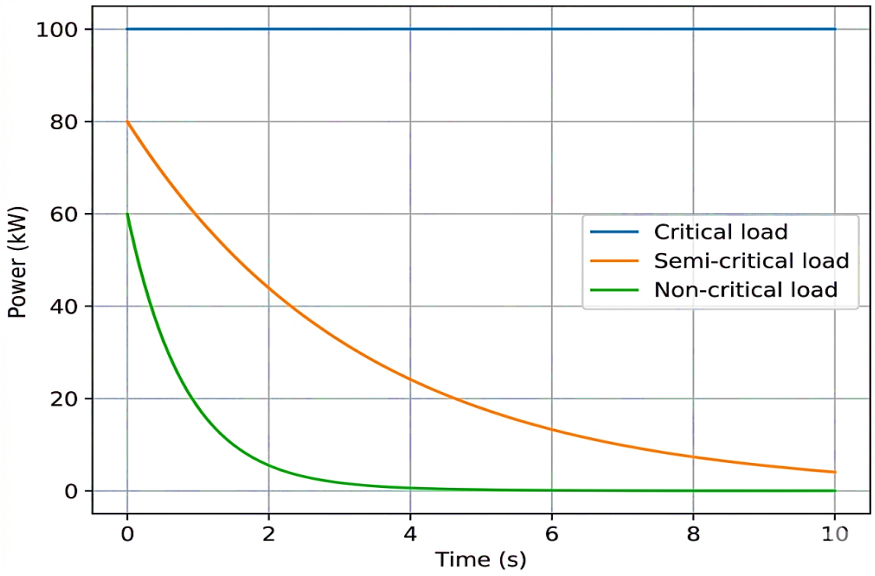


Figure 10. Load shedding profile.

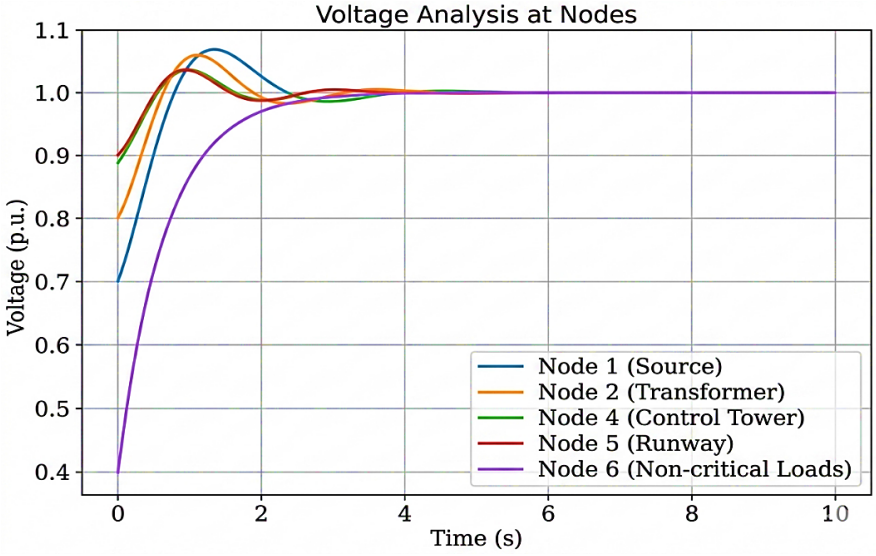


Figure 11. Nodal voltage analysis.

3.8. Nodal Voltage Analysis

Nodal voltage analysis allows for the assessment of power supply quality at various

points in the grid, identifying areas sensitive to voltage fluctuations. Figure 11 presents the voltage evolution at different strategic nodes of the airport power system.

4. Discussions

The integration of voltage-dependent exponential load models (Equations (8) - (11)) within a Differential-Algebraic Equation (DAE) framework enables a critical analysis of the resilience of Ndjili International Airport. The numerical results materialize the technological bottlenecks associated with operating a microgrid in forced islanded mode.

The examination of the steady-state power balance (Table 1 and Figure 6) reveals a critical asymmetry in the infrastructure's power flow distribution. Node (N7) (Commercial & Services) alone accounts for *623.8 kW*, representing approximately *74%* of the total active load, excluding losses, of the 400 V terminal distribution network. This hyper-concentration accentuates grid vulnerability during the transition to backup sources.

The calculated losses at node N7 reach 10%, reflecting a manifest sub-optimality in the low-voltage cabling structure or an under-sizing of the conductors supplying the commercial zone. Conversely, node N2 (Main MV/LV Transformer) displays a loss rate of 1.2%, which complies with industrial standards for machines within this power class.

The total installed capacity of the backup generators (N9 = 1428 kW/1053.15 kVAr) theoretically offers a redundancy factor of 1.7 relative to the overall site demand of 842.6 kW. The infrastructure thus possesses a sufficient power margin under nominal configuration, ensuring that complete islanding is not accompanied by an immediate static collapse.

The time-domain voltage profiles (Figure 7, Figure 8, and Figure 11) highlight the behavior of the automatic voltage regulator (AVR) control system during the loss of the SNEL main grid. At $t = 5$ s (Figure 7), the disconnection from SNEL causes an instantaneous drop in nodal voltage to 0 pu during the switching delay and no-load startup of the alternators. Upon generator connection at $t = 7$ s, the subtransient impedance Z_g initially restricts the terminal voltage to 0.78 pu at node N6 (Figure 11), inducing a high inrush current.

The voltage restoration kinetics (Figure 7) show a convergence toward 1.0 pu in approximately 4.5 seconds ($t = 11.5$ s). This response time is governed by the excitation block time constant (T_A). The absence of any major overshoot in the overall voltage (Figure 7) validates the gain setting (KA), avoiding transient overvoltages that would be destructive to the control tower electronics (N5).

The combined failure scenario (Figure 8) highlights the physical limitations of the current redundancy. The simultaneous loss of the main grid and Diesel Generator 3 (640 kW) reduces the available backup capacity to only 788 kW (DG1 + DG2). This capacity proves to be lower than the overall site load prior to load shedding (842.6 kW).

Under these conditions (Figure 8), the voltage collapses again at $t = 12$ s because the system, despite AVR action, enters voltage instability due to overloading. This proves that the long-term resilience of Ndjili Airport cannot rely solely on a passive load-shedding logic, but requires the integration of dynamic dispatching systems or new injection sources.

The interaction between the mechanical power of the diesel engines and the dynamic load is illustrated through the frequency analysis (Figure 9) and the load shedding profile (Figure 10).

Upon the initial step load impact at $t = 0$ s in Figure 9, the frequency drops sharply to 48.5 Hz. This value precisely coincides with the threshold of the Under-Frequency Load Shedding (UFLS) relay, which is configured to preserve the structural integrity of the generator shafts. This frequency nadir is attributed to the low combined inertia of the three alternators when subjected to simultaneous load connections.

The oscillatory behavior of the frequency exhibits a primary peak at 50.5 Hz ($t = 1$ s) before stabilizing at the nominal value of *50 Hz* within 4 seconds. The damping ratio (ξ) (Equation (26)) proves sufficient to damp the underdamped pseudo-periodic oscillations, thereby confirming the robust performance of the diesel engine speed governors.

Figure 10 quantitatively validates the selective load shedding policy. Non-critical loads decay almost exponentially immediately following the onset of the disturbance, instantaneously releasing active power reserves. This rapid action protects the critical load, which remains strictly stable at 100% of its nominal power throughout the transient state, thus validating the implemented energy control logic.

A detailed analysis of Figure 11 demonstrates the effectiveness of the UPS systems (N8) dedicated to the critical nodes (N4) (Runway Lighting) and (N5) (Control Tower). Their respective voltages exhibit limited transient excursions (>0.9 pu), ensuring strict compliance with ICAO Category I requirements, whereas node (N6) experiences a prolonged voltage sag below the 0.85 pu threshold.

The obtained results indicate that source redundancy is critical to guaranteeing electrical availability within a sensitive airport environment. The implementation of a dedicated transformer and supplementary generators significantly enhances fault tolerance.

The incident reported in September 2025 illustrates the vulnerability of the Ndjili Airport electrical system, where a prolonged power outage led to the suspension of critical airfield operations, including runway lighting and control tower functions. This event highlights the insufficiency of the existing backup systems and emphasizes the necessity for a more robust energy strategy.

Several optimization measures are proposed:

- Implementation of an Energy Management System (EMS): Optimizes load allocation and distribution.
- Adequate Sizing of Backup Generators: Integrates high-performance Uninter-

ruptible Power Supplies (UPS).

- Deployment of Local Renewable Energy Sources: Utilizes solar and hybrid generation systems.
- Internal Grid Segmentation: Isolates critical loads during fault conditions.

5. Conclusions

Systemic analysis and Newton-Raphson power flow modeling of the Ndjili International Airport (Kinshasa, DRC) microgrid quantified the intrinsic limitations of its current configuration when subjected to grid instability from the public utility (SNEL). Source redundancy is essential to maintaining power continuity for critical loads. Although the thermal backup infrastructure, with a nominal capacity of 1428 kW, is theoretically oversized to cover the global isolated site load of 842.6 kW, the dynamic Differential-Algebraic Equation (DAE) approach highlighted a critical vulnerability during N1 contingency scenarios (simultaneous loss of the main grid and Generator 3).

Time-domain simulations demonstrate that the voltage and frequency stability of the hub depends exclusively on the control kinetics of the Automatic Voltage Regulator AVR (T_A = 0.08 s) and the alternator speed governors. Although the automated under-frequency/under-voltage load shedding (UFLS/UVLS) strategy effectively prioritizes the preservation of vital loads (Control Tower, Runway Lighting), a recurrent voltage collapse at t = 12 s under severe contingency conditions proves the urgent need for a transition toward an active, decentralized architecture.

Active energy management strategies constitute a key lever for electrical system performance. The adoption of an Energy Management System (EMS) would enable real-time flow monitoring, fault anticipation, and effective coordination of the transfer between primary and backup sources.

Long-term planning must include the integration of solar photovoltaic (PV) sources to reduce dependence on the public grid and reinforce the airport's energy resilience. A hybrid approach combining the utility grid, diesel generators, and solar energy could provide a sustainable and economically viable solution.

Operational reliability and safety cannot be guaranteed without a rigorous preventive maintenance program and continuous training of technical teams in electrical system management and emergency protocols. Implementing Key Performance Indicators (KPIs) such as availability rate, Mean Time to Recovery (MTTR), and energy losses is essential to evaluating the effectiveness of the deployed measures.

The results of this study demonstrate that the resilience of an airport electrical system depends as much on equipment quality as on the energy management strategy. The findings obtained for Ndjili Airport can serve as a benchmark model for other airports in similar contexts, where grid instability and load criticality make the design of robust, flexible systems imperative. The proposed recommendations aim to reinforce safety, energy efficiency, and operational continuity, while provid-

ing a methodological framework for future optimization and modernization studies of airport electrical infrastructures.

Author Contributions

Professor Anthony Bassesuka Sandoka Nzao supervised doctoral students Benjamin Ndubu Khonde and Tuka Biaba Samuel Garcia. He contributed to developing the scientific content, shaping the formal presentation of the subject, and defining, organising, and verifying the methodology using Newton-Raphson analysis.

Doctoral students Benjamin Ndubu Khonde and Tuka Biaba Samuel Garcia performed the modelling and numerical simulations. They also analysed the results and helped prepare the manuscript. All authors contributed to critically revising the work and validating the final version.

This wording aligns better with the terminology used in international publications: conceptualisation, methodology, validation, analysis of results, and drafting and critical revision of the manuscript.

Conflicts of Interest

The authors declare no conflicts of interest regarding the publication of this paper.

References

[1] Ackermann, T., Andersson, G. and Söder, L. (2001) Distributed Generation: A Definition. *Electric Power Systems Research*, **57**, 195-204. https://doi.org/10.1016/s0378-7796(01)00101-8

[2] Bollen, M. and Hassan, F. (2011) Integration of Distributed Generation in the Power System. Wiley. https://doi.org/10.1002/9781118029039

[3] Bollen, M.H.J. (2000) Understanding Power Quality Problems: Voltage Sags and Interruptions. IEEE Press. https://books.google.com.br/books?id=Je0eAQAAIAAJ

[4] Chow, J.H. (2013) Introduction. In: *Power System Coherency and Model Reduction*, Springer, 1-14. https://doi.org/10.1007/978-1-4614-1803-0_1

[5] De la Ree, J., Varma, R. and Toussaint, M. (2000) Power System Synchronizing and Damping Torque Coefficient Estimation Using PMU Data. *Proceedings of the IEEE PES General Meeting*, Seattle, WA, 16-20 July 2000, 1111-1116.

[6] El-Hawary, M.E. (2008) Electrical Power Systems: Design and Analysis. John Wiley & Sons. https://books.google.com/books/about/Electrical_Power_Systems.html?id=Z0BHpnMMfwQC

[7] El-Saadany, E. and Salama, M.M.A. (1999) Distributed Generation Technologies, Definitions and Benefits. *Electric Power Systems Research*, **71**, 119-128. https://www.sciencedirect.com/science/article/pii/S0378779604000240

[8] IEEE Power & Energy Society (2006) IEEE Standard Definitions for Use in Reporting Electric Generating Unit Reliability (IEEE Std 762-2006). IEEE. https://standards.ieee.org/ieee/762/3639/

[9] Agence Congolaise de Presse (2025) Aéroport de Ndjili dans le noir: La RVA est l'unique responsable. https://acp.cd/nation/aeroport-de-ndjili-dans-le-noir-la-rva-est-lunique-responsable/

[10] Agence Congolaise de Presse (2025) Aéroport international de N'djili: L'installation d'un nouveau transformateur électrique envisagée. https://acp.cd/nation/aeroport-de-ndjili-linstallation-dun-nouveau-transformateur-electrique-envisagee/

[11] AllAfrica (2025) Congo-Kinshasa: Les sanctions tombent après la panne de courant à l'aéroport de Kinshasa-Ndjili. https://fr.allafrica.com/stories/202509130071.html

[12] FoxTime.cd (2025) Kinshasa: L'aéroport de Ndjili doté d'un nouveau transformateur de 15 MVA, une réponse solide à l'incident du 10 septembre. https://foxtime.cd/kinshasa-laeroport-de-ndjili-dote-dun-nouveau-transformateur-de-15-mva-une-reponse-solide-a-lincident-du-10-septembre/

[13] Ministère des Transports—RDC (2024) Rapport national sur la performance des infrastructures aéroportuaires (section énergie et réseaux). Ministère des Transports. https://www.transports.gouv.cd/

[14] Kundur, P. and Malik, O.P. (2022) Power System Stability and Control. 2nd Edition, McGraw-Hill Education. https://www.mhprofessional.com/

[15] Milano, F. (2022) Advances in Power System Modelling, Control and Stability Analysis (Energy Engineering). 2nd Edition, The Institution of Engineering and Technology, 764 p. https://www.amazon.com/Advances-Modelling-Stability-Analysis-Engineering-dp-183953575X/dp/183953575X/ref=dp_ob_title_bk

[16] Glover, J.D., Overbye, T.J. and Sarma, M.S. (2024) Power System Analysis and Design. 7th Edition, Cengage Learning. https://www.cengage.com/

[17] National Academies of Sciences, Engineering, and Medicine (2023) Airport Energy Resiliency Roadmap. The National Academies Press.

[18] Bassi, H. and Almutairi, A. (2024) Resilient Microgrids for Critical Infrastructure: Modeling, Control, and Applications. Academic Press.

[19] Bollen, M.H.J. (2025) Power Quality and Reliability in Smart Distribution Grids. Institution of Engineering and Technology. https://digital-library.theiet.org/

[20] Sauer, P.W., Pai, M.A. and Chow, J.H. (2023) Power System Dynamics and Stability: With Synchrophasor Measurement and Advanced Control. 2nd Edition, Wiley.

[21] De-Jesús-Grullón, R., *et al.* (2024) Modeling and Simulation of Distribution Networks with High Renewable Penetration in Open-Source Software: QGIS and OpenDSS. *Energies*, **17**, Article 2925. https://doi.org/10.3390/en17122925

[22] Annaswamy, A.M. and Fradkov, A.L. (2025) Dynamic Load Modeling and Voltage Stability in Isolated Power Systems. Springer.

[23] IEEE (2014) IEEE Recommended Practice for Electric Power Distribution for Industrial Plants (Color Book® Series). IEEE. https://standards.ieee.org/ieee/141/312/

[24] Kundur, P. (1994) Power System Stability and Control. McGraw-Hill. https://books.google.com/

[25] Kundur, P., Balu, N.J. and Lauby, M.G. (1994) Power System Stability and Control. McGraw-Hill.

[26] Li, F., Qiao, W., Sun, H., Wan, H., Wang, J., Xia, Y., *et al.* (2010) Smart Transmission Grid: Vision and Framework. *IEEE Transactions on Smart Grid*, **1**, 168-177. https://doi.org/10.1109/tsg.2010.2053726

[27] Liu, J.-F. and Wang, S.-Y. (2007) Survey on Applications of Wide-Area Measurement System in Power System Analysis. *High Voltage Engineering*, **33**, 182–185. https://www.researchgate.net/publication/298185621_Survey_on_applications_of_wide-area_measurement_system_in_power_system_analysis

[28] Milano, F. (2010) Power System Modelling and Scripting. Springer. https://link.springer.com/book/10.1007/978-3-642-13669-6

[29] Yang, S., Guo, N. and Zhang, S. (2023) Economic Optimization of Microgrid with Demand Response under Source-Load Uncertainty. *Energy Sources*, *Part B*: *Economics*, *Planning*, *and Policy*, **18**, Article 2280591. https://doi.org/10.1080/15567249.2023.2280591

[30] Mwasilu, F., Justo, J.J., Kim, E., Do, T.D. and Jung, J. (2014) Electric Vehicles and Smart Grid Interaction: A Review on Vehicle to Grid and Renewable Energy Sources Integration. *Renewable and Sustainable Energy Reviews*, **34**, 501-516. https://doi.org/10.1016/j.rser.2014.03.031

[31] Samantaray, S.R., *et al.* (2019) Guest Editorial: Intelligent Protection and Control of Microgrids with Energy Storage Integration. *IET Generation*, *Transmission & Distribution*, 1**3**, 741-742.

[32] Pal, B.C. and Chaudhuri, B. (2005) Robust Control in Power Systems. Springer. https://link.springer.com/book/10.1007/b136490

[33] Yadav, S.K., Sharma, N.K. Choube, S.C. and Varma, A. (2017) Optimal Coordination of Overcurrent Relays in Power Systems for Reliability Assessment under the Presence of Distributed Generation Using ETAP. 2017 6*th International Conference on Computer Applications in Electrical Engineering-Recent Advances* (*CERA*), Roorkee, 5-7 October 2017, 51-56. https://doi.org/10.1109/cera.2017.8343300

[34] Pinson, P., Madsen, H., Nielsen, H.A., Papaefthymiou, G. and Klöckl, B. (2008) From Probabilistic Forecasts to Statistical Scenarios of Short-Term Wind Power Production. *Wind Energy*, **12**, 51-62. https://doi.org/10.1002/we.284

[35] Pourmousavi, S.A., Nehrir, M.H. and Sastry, C. (2011). Providing Ancillary Services through Demand Response with Minimum Load Manipulation. 2011 *North American Power Symposium*, Boston, MA, 4-6 August 2011, 1-6. https://doi.org/10.1109/naps.2011.6024876

[36] Yeboah, S.J., Nunoo, S., Attachie, J.C., Asihene, W.D. and Asuamah, E.Y. (2025) Impact and Integration Techniques of Renewable Energy Sources on Smart Grid Operations: A Systematic Review. *Scientific African*, **29**, e02845. https://doi.org/10.1016/j.sciaf.2025.e02845

[37] Chowdhury, A. and Koval, D. (2024) Power Distribution System Reliability: Practical Methods and Applications. 2nd Edition, Wiley. https://www.scirp.org/reference/referencespapers?referenceid=2094380